Increased vessel perfusion predicts the efficacy of immune checkpoint blockade

Xichen Zheng,[1] Zhaoxu Fang,[1] Xiaomei Liu,[1] Shengming Deng,[1] Pei Zhou,[1] Xuexiang Wang,[1] Chenglin Zhang,[2] Rongping Yin,[2] Haitian Hu,[1] Xiaolan Chen,[3] Yijie Han,[4] Yun Zhao,[1] Steven H. Lin,[5] Songbing Qin,[6] Xiaohua Wang,[7] Betty Y.S. Kim,[8] Penghui Zhou,[9] Wen Jiang,[5] Qingyu Wu,[1] and Yuhui Huang[1]

[1]Cyrus Tang Hematology Center, Collaborative Innovation Center of Hematology, State Key Laboratory of Radiation Medicine and Prevention, and [2]School of Nursing, Soochow University, Suzhou, Jiangsu, China. [3]Institute of Pediatric Research, Affiliated Children's Hospital of Soochow University, Suzhou, Jiangsu, China. [4]Key Laboratory of Protein and Peptide Pharmaceuticals, Institute of Biophysics, Chinese Academy of Sciences, Beijing, China. [5]Department of Radiation Oncology, University of Texas MD Anderson Cancer Center, Houston, Texas, USA. [6]Department of Radiotherapy, and [7]First Affiliated Hospital of Soochow University, Suzhou, Jiangsu, China. [8]Department of Neurosurgery, Mayo Clinic, Jacksonville, Florida, USA. [9]State Key Laboratory of Oncology in Southern China, Sun Yat-Sen University Cancer Center, Guangzhou, Guangdong, China.

Immune checkpoint blockade (ICB) has demonstrated curative potential in several types of cancer, but only for a small number of patients. Thus, the identification of reliable and noninvasive biomarkers for predicting ICB responsiveness is an urgent unmet need. Here, we show that ICB increased tumor vessel perfusion in treatment-sensitive EO771 and MMTV-PyVT breast tumor as well as CT26 and MCA38 colon tumor models, but not in treatment-resistant MCaP0008 and 4T1 breast tumor models. In the sensitive tumor models, the ability of anti–cytotoxic T lymphocyte–associated protein 4 or anti–programmed cell death 1 therapy to increase vessel perfusion strongly correlated with its antitumor efficacy. Moreover, globally enhanced tumor vessel perfusion could be detected by Doppler ultrasonography before changes in tumor size, which predicted final therapeutic efficacy with more than 90% sensitivity and specificity. Mechanistically, $CD8^+$ T cell depletion, IFN-γ neutralization, or implantation of tumors in IFN-γ receptor knockout mice abrogated the vessel perfusion enhancement and antitumor effects of ICB. These results demonstrated that ICB increased vessel perfusion by promoting $CD8^+$ T cell accumulation and IFN-γ production, indicating that increased vessel perfusion reflects the successful activation of antitumor T cell immunity by ICB. Our findings suggest that vessel perfusion can be used as a novel noninvasive indicator for predicting ICB responsiveness.

Introduction

Recent advances in cancer immunotherapy have revolutionized cancer treatment. Immune checkpoint blockade (ICB), designed to target immune suppressive signals such as cytotoxic T lymphocyte–associated protein 4 (CTLA4) or programmed cell death 1 (PD1), has produced durable responses in some patients with advanced-stage and treatment-refractory cancers, including melanoma, non–small cell lung cancer, renal cell carcinoma, and Merkel cell carcinoma (1–5). However, despite these exciting results, only about one-quarter of patients experience a benefit from ICB monotherapy (2–4, 6). Therefore, novel strategies are needed to identify likely ICB responders to improve therapeutic efficacy.

Various tissue-based biomarkers have been explored to identify which patients are likely to respond to ICB. For instance, an increase in the ratio of tumor-infiltrating $CD8^+$ cytotoxic T cells over regulatory T cells (Tregs) was linked to response to anti–CTLA4 therapy (4, 7). Greater infiltration of $CD8^+$ T cells that express PD1 or programmed cell death protein ligand 1 (PD-L1) was associated with a better response to PD1 signaling blockade (3, 6). Likewise, PD-L1 expression was proposed as a promising biomarker to predict the effectiveness of anti–PD1 therapy (6, 8–10). Finally, mutational load is known to prompt the production of neoantigens for immune cells to recognize cancer cells, and has been linked to positive responses to ICB in the clinic (11, 12). Although a correlation between genetic mutations and ICB responsiveness could be used to estimate overall response rates in different cancer types, this may not be useful for individual patients (3, 11, 12). Moreover, these tissue-based methods can provide a baseline assessment of tumor immunogenicity, but are not suitable for longitudinal monitoring of changes in the tumor microenvironment (TME) over time during the course of treatment.

The task of identifying a noninvasive and reliable biomarker of responsiveness to ICB is further complicated by the fact that the response of tumors to immunotherapy differs from their response to chemotherapy and radiotherapy (2, 3). Pseudoprogression of lesions during ICB limits the classification of lesion size as a direct correlation of treatment responses (13, 14). In this case, the ability to discern real-time physiological changes within the TME is more critical than lesion size in assessing actual antitumor immunity. Therefore, we proposed to identify TME-based

Authorship note: XZ and ZF contributed equally to this work.
Conflict of interest: The authors have declared that no conflict of interest exists.
Submitted: July 28, 2017; **Accepted:** March 1, 2018.
Reference information: *J Clin Invest*. 2018;128(5):2104–2115.
https://doi.org/10.1172/JCI96582.

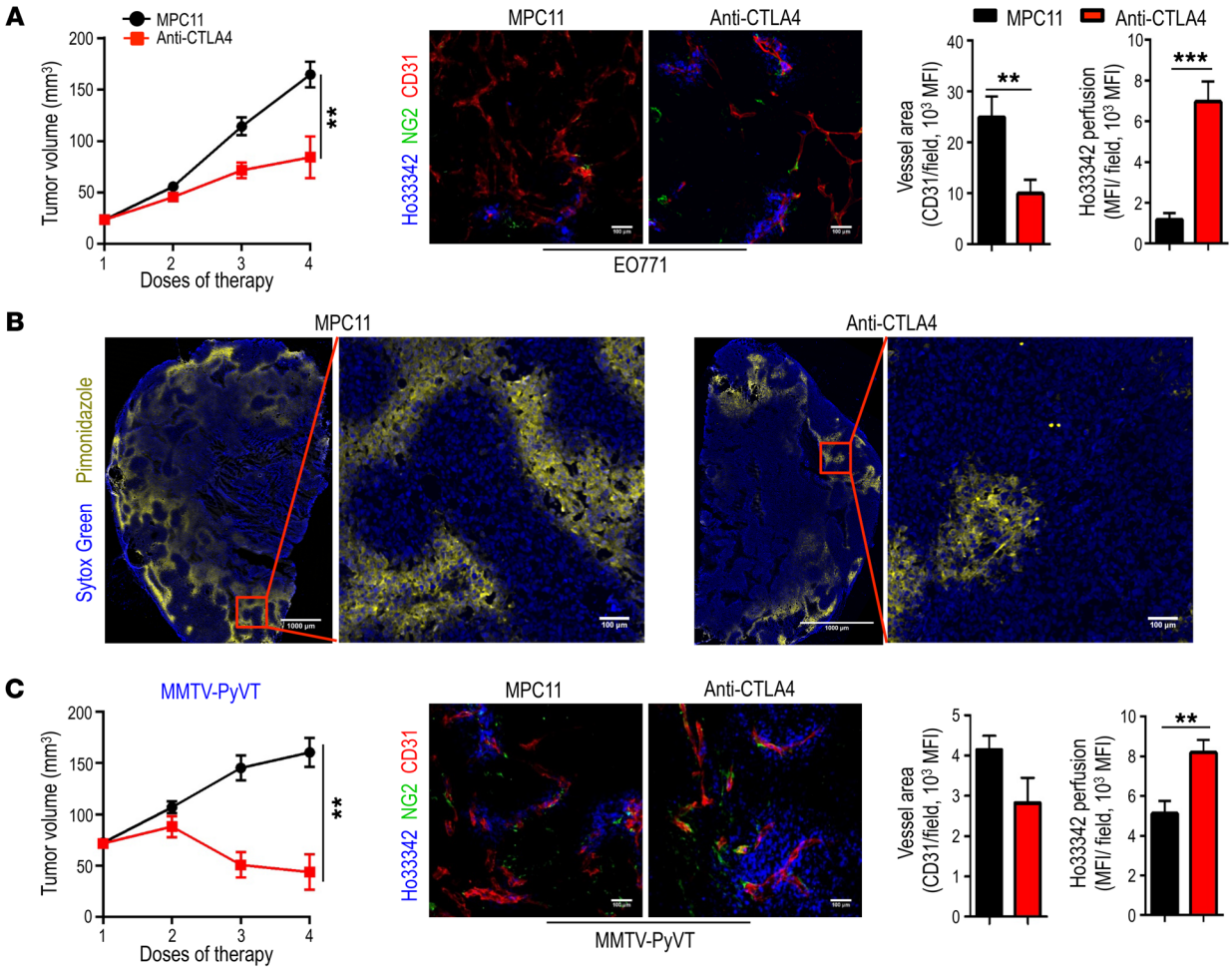

Figure 1. ICB increases tumor vessel perfusion in treatment-sensitive, but not treatment-resistant, breast tumor models. Mice bearing orthotopic breast tumors (MMTV-PyVT, EO771, 4T1, or MCaP0008) were treated with an anti–CTLA4 antibody or an isotype-matched control antibody (MPC11) every 3 days for a total of 4 doses; tumor size was measured every 3 days. Vessel perfusion of tumor tissues was assessed by confocal microscopy. (**A**) Anti–CTLA4 therapy inhibited tumor growth and increased vessel perfusion in EO771 breast tumors. Scale bars: 100 μM. (**B**) Anti–CTLA4 therapy reduced tumor tissue hypoxia in EO771 breast tumors. Scale bars: 1,000 or 100 μM. (**C**) Anti–CTLA4 therapy induced tumor regression and improved vessel perfusion in MMTV-PyVT breast tumors. Scale bars: 100 μM. MFI, mean fluorescence intensity; Ho33342 (blue), Hoechst 33342 perfused area; CD31 (red), endothelial cells; NG2 (green), pericytes; and Sytox Green (green), counterstained for tumor tissue. Significance was determined by unpaired 2-tailed Student's *t* tests. Data are from 1 experiment representative of 3 independent experiments with similar results (n = 8–10 mice per group in **A** and **B**; n = 7–8 mice per group in **C**). All data are mean ± SEM. $^{**}P < 0.01$, $^{***}P < 0.001$.

pathophysiological variables with the potential to reflect both the overall and dynamic antitumor immunity induced by ICB. By using several clinically relevant mouse models, including orthotopic (EO771, 4T1, and MCaP0008) and spontaneous (MMTV-PyVT) breast tumor models that mirror cancer progression in humans, we found that both anti–CTLA4 and anti–PD1 agents enhanced tumor vessel perfusion and that this enhancement correlated strongly with the antitumor efficacy of the agents. We further demonstrated that the enhanced vessel perfusion and antitumor effects of ICB shared a key underlying mechanism through the activation of $CD8^+$ T cells. Finally, we used Doppler ultrasonography to show that the overall increase in perfusion induced by ICB could be measured before tumor size changes and could efficiently predict individual tumor responsiveness. Together, our findings identify a novel strategy to precisely determine responsiveness to ICB agents at an early stage of treatment.

Results

ICB increases tumor vessel perfusion in treatment-sensitive tumors. To explore TME-based variables that reflect different responses to ICB agents, we treated 4 representative breast tumor models with an anti–CTLA4 antibody and found that the orthotopic EO771 and genetically engineered MMTV-PyVT spontaneous breast tumor models were ICB sensitive, whereas the MCaP0008 and 4T1 models were ICB resistant (Figure 1 and Supplemental Figure 1; supplemental material available online with this article; https://doi.org/10.1172/JCI96582DS1). The difference in response of these models to ICB is consistent with previous reports of their immunogenicity (15–19). Some intrinsic properties of tumor tissue likely determine whether a tumor will respond to ICB. Previous work has demonstrated that tumor vascular normalization alleviates the immunosuppressive TME and improves cancer immunotherapy (16, 20–23). We there-

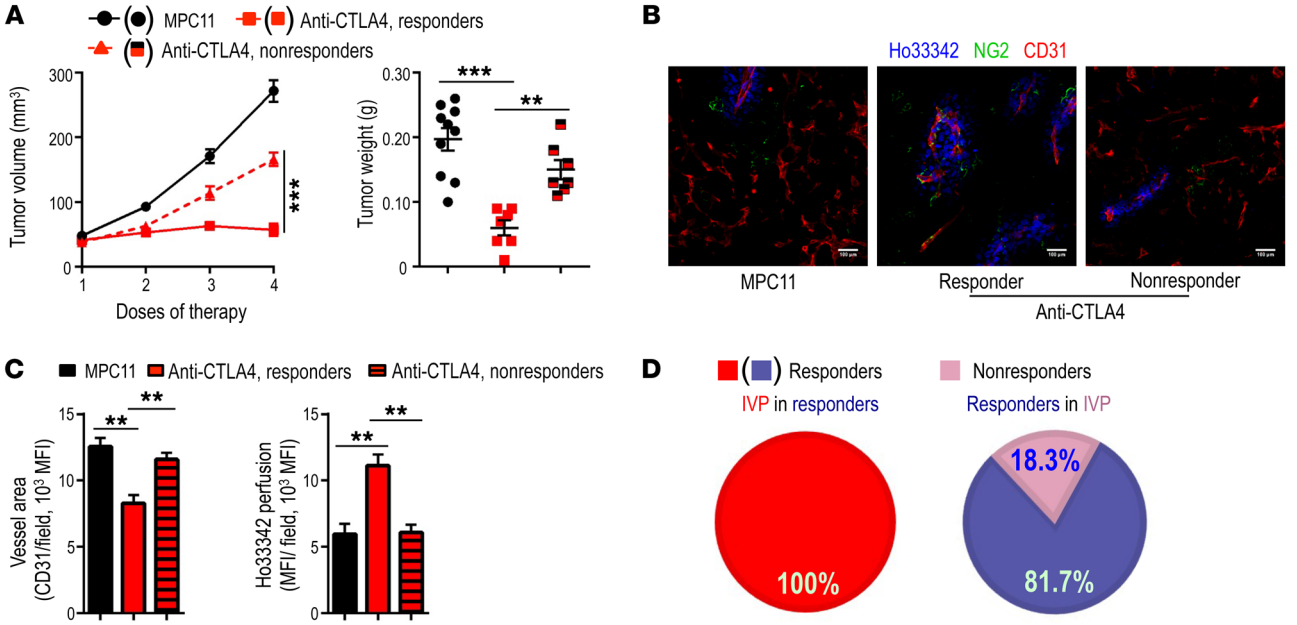

Figure 2. IVP correlates with the antitumor effectiveness of CTLA4 blockade. (**A**) EO771 tumors were stratified as responders or nonresponders according to whether 4 doses of anti–CTLA4 therapy stopped their progression or not. (**B** and **C**) Anti–CTLA4 therapy increased tumor vessel perfusion in responders, but not nonresponders, of EO771 tumors (n = 10–14 mice per group). Scale bars: 100 μM. (**D**) IVP was observed in 100% of responder tumors. Among the EO771 tumors treated with anti–CTLA4 therapy and assessed for vessel perfusion (122 mice total), 49 were responders and 60 had increased vessel perfusion. Significance was determined by 1-way ANOVA with Bonferroni's adjusted post hoc t tests for multiple comparisons (**A** and **C**). Data are from 1 experiment representative of 3 independent experiments (**A**–**C**), or are pooled from multiple independent experiments (**D**). $^{**}P < 0.01$, $^{***}P < 0.001$.

fore hypothesized that the effectiveness of ICB might be determined by its ability to remodel the TME to counteract overall immunosuppression. In accordance with this hypothesis, we observed that anti–CTLA4 therapy reduced tumor vessel density, increased pericyte coverage, enhanced vessel perfusion, and reduced tissue hypoxia in treatment-sensitive EO771 breast tumors (Figure 1, A and B, and Supplemental Figure 1, A and B), indicating that anti–CTLA4 therapy itself can induce tumor vascular normalization, consistent with a recent report (19). Anti–CTLA4 therapy also induced vascular normalization in the treatment-sensitive MMTV-PyVT breast tumor model, but not in the treatment-resistant MCaP0008 and 4T1 models (Figure 1C and Supplemental Figure 1, C–E). Tumor vascular normalization refers to a process in which the tumor vasculature is remodeled to more closely resemble that of normal tissue vessels, and increased vessel perfusion (IVP) is a critical component of this process (20, 24, 25). Here, we found that IVP correlated strongly with the responsiveness of a tumor to anti–CTLA4 therapy (Figure 1 and Supplemental Figure 1). We extended this study to other immune checkpoint blocking agents and observed that an anti–PD1 antibody also resulted in IVP in EO771 and MMTV-PyVT tumors (Supplemental Figures 2 and 3). Similarly, anti–CTLA4 therapy also enhanced vessel perfusion in its respective canonical CT26 colon cancer model (Supplemental Figure 4). In contrast, anti–CTLA4 therapy did not affect blood vessels in normal tissues, e.g., colon tissue (Supplemental Figure 5). These results demonstrate that ICB increases tumor vessel perfusion in several types of solid tumors and that this effect can distinguish ICB-sensitive from ICB-resistant tumors.

IVP by ICB therapy correlates with antitumor efficacy. These findings prompted us to test whether IVP can predict responsiveness to ICB. In a survival mouse study with EO771 tumors, we observed that tumors that stopped progressing after 4 cycles of anti–CTLA4 treatment would show a complete antitumor response. Conversely, if a tumor continued to progress after 4 cycles of anti–CTLA4 treatment, that tumor would become therapy resistant (Supplemental Figure 6A). On the basis of these results, we stratified individual EO771 tumors as responding or nonresponding (Figure 2A) and found that the overall response rate of EO771 tumors to anti–CTLA4 therapy was 34.7% (74 responders among 213 mice), a value comparable to the reported response rate to ipilimumab in patients with melanoma (26). Histologic analysis showed a significant increase in tumor vessel perfusion in anti–CTLA4 therapy–responsive tumors compared with those in the isotype control group or nonresponders (Figure 2, B and C). Moreover, using the mean value of vessel perfusion as a cutoff to distinguish tumors as IVP versus non-IVP in the anti-CTLA4–treated group, we found that all 49 responsive tumors exhibited the IVP phenotype (sensitivity = 100%), whereas only 11 of the 60 tumors classified as IVP phenotype were nonresponders (18.3%) (Figure 2D). In anti–PD1 therapy, the treatments promoted the infiltration and activation of $CD8^+$ T cells, inhibited tumor growth, and increased vessel perfusion in MCA38 colon tumor, compared with those in the isotype control group (Figure 3, A–D). Notably, 32 of the total 36 MCA38 tumors were responsive to anti–PD1 therapy. Compared with the mean value of vessel perfusion in the control group, we found that 29 of the 32 responding tumors displayed an IVP phenotype (sensitivity = 90.6%) (Figure 3E). Among the 36 tumors, all of the 29

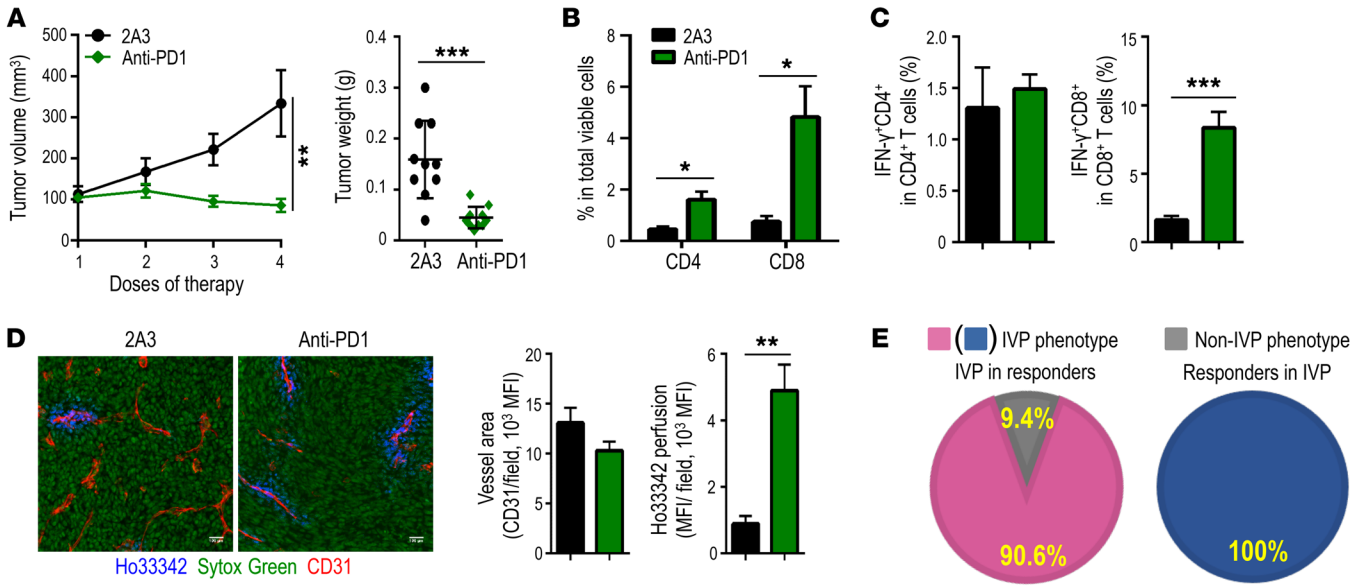

Figure 3. IVP by anti–PD1 therapy positively correlates with antitumor efficacy. When MCA38 colon tumors reached 5–6 mm in diameter, mice were randomly assigned to 2 groups and treated with an anti–PD1 antibody (10 mg/kg) or an isotype-matched control antibody (2A3) for 3–4 doses every 3 days. (**A**) Anti–PD1 therapy induced regression of MCA38 tumors. (**B** and **C**) Anti–PD1 therapy increased intratumoral CD4⁺ and CD8⁺ T cells, and promoted IFN-γ production in CD8⁺ T cells. (**D**) Anti–PD1 treatments increased tumor vessel perfusion without affecting vessel density. Scale bars: 100 μM. (**E**) Increased vessel perfusion was observed in 90.6% of responding tumors. Among the 36 MCA38 tumors treated with an anti–PD1 antibody, 32 were responders and 30 had increased vessel perfusion. Significance was determined by unpaired 2-tailed Student's *t* tests. Data are from 1 experiment representative of 3 independent experiments (**A**–**D**, $n = 10$ mice per group), or are pooled from multiple independent experiments (**E**). $^*P < 0.05$, $^{**}P < 0.01$, $^{***}P < 0.001$.

tumors classified as IVP phenotype were responders (100%) (Figure 3E). Together, these results suggest that IVP may be a sensitive parameter for identifying ICB-responsive tumors.

The vascular remodeling and antitumor effects of ICB depend on CD8⁺ T cells. Because enhanced vessel perfusion was observed mostly in treatment-sensitive tumors, we proposed that ICB therapy enhances tumor vessel perfusion through a mechanism that also underlies its antitumor effects. A significant increase in intratumoral CD8⁺ T cells was observed in anti-CTLA4–responsive EO771 tumors, but not in 4T1 or anti-CTLA4–nonresponsive EO771 tumors (Supplemental Figure 6, B and C, and Supplemental Figure 7). To test whether T cells are responsible for the effects of CTLA4 blockade on tumor growth and vessel perfusion, we performed in vivo depletion of CD4⁺ and CD8⁺ T cells in tumor-bearing mice. This simultaneous depletion of CD4⁺ and CD8⁺ T cells completely negated the IVP phenotype and inhibition of tumor growth induced by anti–CTLA4 therapy (Figure 4, A–D). Consistently, such depletion also eliminated the transcription of genes related to antitumor immunity and angiostasis, including *Ifng*, *Cxcl9*, and *iNos* (Figure 4E). These observations were also consistent with the depletion of only CD8⁺ T cells (Figure 5). In contrast, in vivo depletion of only CD4⁺ T cells had the opposite effect. Depletion of only CD4⁺ T cells increased tumor vessel perfusion and inhibited tumor growth as compared with the control group, which was comparable to anti–CTLA4 monotherapy (Figure 5). We also depleted CD8⁺ T cells in the MCA38 tumor model with anti–PD1 therapy, which led to a similar reversal of the tumor growth inhibition and the vessel perfusion improvement induced by anti–PD1 therapy (Figure 6). Together, these findings suggest that CD8⁺ T lymphocytes mediate both IVP and inhibition of tumor growth by ICB therapy, and that CD4⁺ T lymphocytes negatively regulate these effects.

We also assessed the interplay between CD4⁺ and CD8⁺ T cells. In vivo depletion of only CD8⁺ T cells did not affect tumor accumulation of CD4⁺ T cells, but did reduce their IFN-γ production (Figure 5B and Supplemental Figure 8, A and C). Conversely, depletion of only CD4⁺ T cells promoted tumor accumulation of CD8⁺ T cells and elevated IFN-γ production (Figure 5B and Supplemental Figure 8, B and D). The most prominent increase in tumor accumulation of CD8⁺ T cells occurred when CD4⁺ T cells were depleted in combination with anti–CTLA4 treatment (Figure 5B and Supplemental Figure 8, B and D). These findings further support that ICB therapy affects tumor growth and vessel perfusion via CD8⁺ T cells, an effect that is antagonized by CD4⁺ T cells.

IFN-γ mediates the effects of anti–CTLA4 therapy on vessel perfusion and tumor growth. We then investigated how T cells mediate the vascular remodeling induced by anti–CTLA4 therapy. By analyzing the transcription of angiogenic and angiostatic genes in tumor tissues, we found that anti–CTLA4 therapy upregulated the mRNA levels of angiostatic genes *Ifng* and *Cxcl9*, without affecting the mRNA levels of common angiogenic factors, such as vascular endothelial growth factor, placental growth factor, and fibroblast growth factor (Supplemental Figure 9, A and B). Anti–PD1 therapy also increased *Ifng* and *Cxcl9* expression (Supplemental Figure 9C). Together with the finding that anti–CTLA4 therapy elevated IFN-γ expression in CD8⁺ T cells (Supplemental Figure 8D) and the fact that IFN-γ is a key mediator of antitumor immunity with angiostatic activity (27–30), we hypothesized that IFN-γ is critical for vessel modulation after

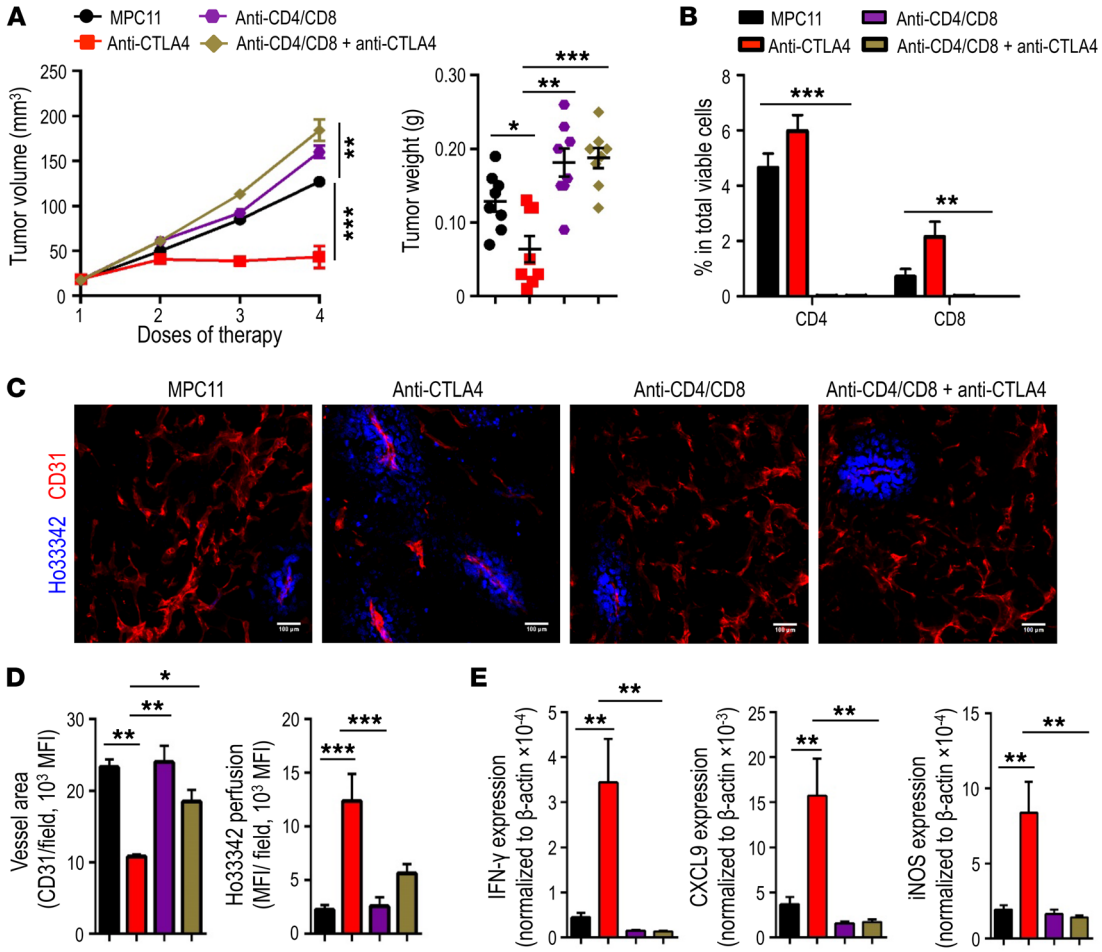

Figure 4. In vivo depletion of T cells reverses IVP and the inhibition of tumor growth induced by anti–CTLA4 therapy. When EO771 breast tumors reached 3–4 mm in diameter, mice were randomly assigned to 4 groups and treated with anti–CD8 and anti–CD4 antibodies, or isotype 2A3 antibody (200 μg/mouse each) on days 0, 2, and 8. On day 1, mice were further treated with an anti–CTLA4 antibody or MPC11 (5 mg/kg) every 3 days for 4 doses. (**A**) In vivo depletion of $CD8^+$ and $CD4^+$ T cells completely eliminated the antitumor effect of anti–CTLA4 therapy. (**B**) Anti–CD8 and anti–CD4 antibody coadministration eradicated tumor-infiltrating T cells. (**C** and **D**) In vivo depletion of $CD8^+$ and $CD4^+$ T cells reversed IVP induced by anti–CTLA4 therapy. Scale bars: 100 μM. (**E**) In vivo depletion of $CD8^+$ and $CD4^+$ T cells abolished the effects of anti–CTLA4 therapy on the transcription of genes related to antitumor immunity. Significance was determined by 1-way ANOVA with Bonferroni's adjusted post hoc *t* tests for multiple comparisons. Data are from 1 experiment representative of 2 independent experiments (n = 8–10 mice per group). $^*P < 0.05$, $^{**}P < 0.01$, $^{***}P < 0.001$.

CTLA4 blockade. Indeed, neutralizing IFN-γ in vivo abolished the anti-CTLA4–induced phenotypes in vessel perfusion, tumor growth, and the tumor accumulation of $CD8^+$ T cells (Supplemental Figure 10). This is consistent with in vivo depletion of T cells, which eliminated the effect of anti–CTLA4 therapy on *Ifng* expression (Figure 4E). We also found that in IFN-γ receptor knockout (IFN-$\gamma R^{-/-}$) mice, anti–CTLA4 therapy had little effect on tumor growth and tumor vessel perfusion, compared with WT mice (Figure 7). These findings suggest that IFN-γR signaling is required for the vascular remodeling and tumor growth inhibition in anti–CTLA4 therapy.

Anti–CTLA4 therapy increases vessel perfusion before noticeable tumor size changes. The finding that activated T cells mediate the ICB effects on both IVP and tumor growth inhibition suggests that IVP is an ICB-induced alteration that in turn facilitates ICB antitumor efficacy, or a consequence of ICB-induced tumor regression. To clarify this issue, we performed a time-course study in which EO771 tumors were harvested on days 3, 6, and 9 after treatment with anti–CTLA4 or isotype-matched control antibody (MPC11). Because the TME is heterogeneous, we analyzed overall tumor vessel perfusion in cross sections of entire tumor tissues. In the MPC11 control group, the vessel perfusion per tumor area was similar over time, whereas tumor sizes consistently and significantly increased (tumor weights: day 3 = 0.051 ± 0.0058 g, day 6 = 0.089 ± 0.0088 g, and day 9 = 0.15 ± 0.012 g; day 3 vs. day 6, $P = 0.0031$; day 6 vs. day 9, $P = 0.0007$) (Figure 8). In contrast, in the anti-CTLA4–treated group, the vessel perfusion per tumor area persistently and significantly increased over time (vessel perfusion [MFI/μm²]: day 3 = 0.0076 ± 0.00082, day 6 = 0.024 ± 0.0061, and day 9 = 0.062 ± 0.0062; day 3 vs. day 6, $P = 0.032$; day 6 vs. day 9, $P = 0.0002$), whereas tumor sizes remained similar (tumor weight: day 3 vs. day 6, $P = 0.546$; day 6 vs. day 9, $P = 0.989$) (Figure 8). These findings show that anti–CTLA4 therapy increases tumor vessel perfusion in a time-dependent manner before tumor size changes are detectable, supporting the idea that IVP may serve as a predictive indicator for the treatment responsiveness.

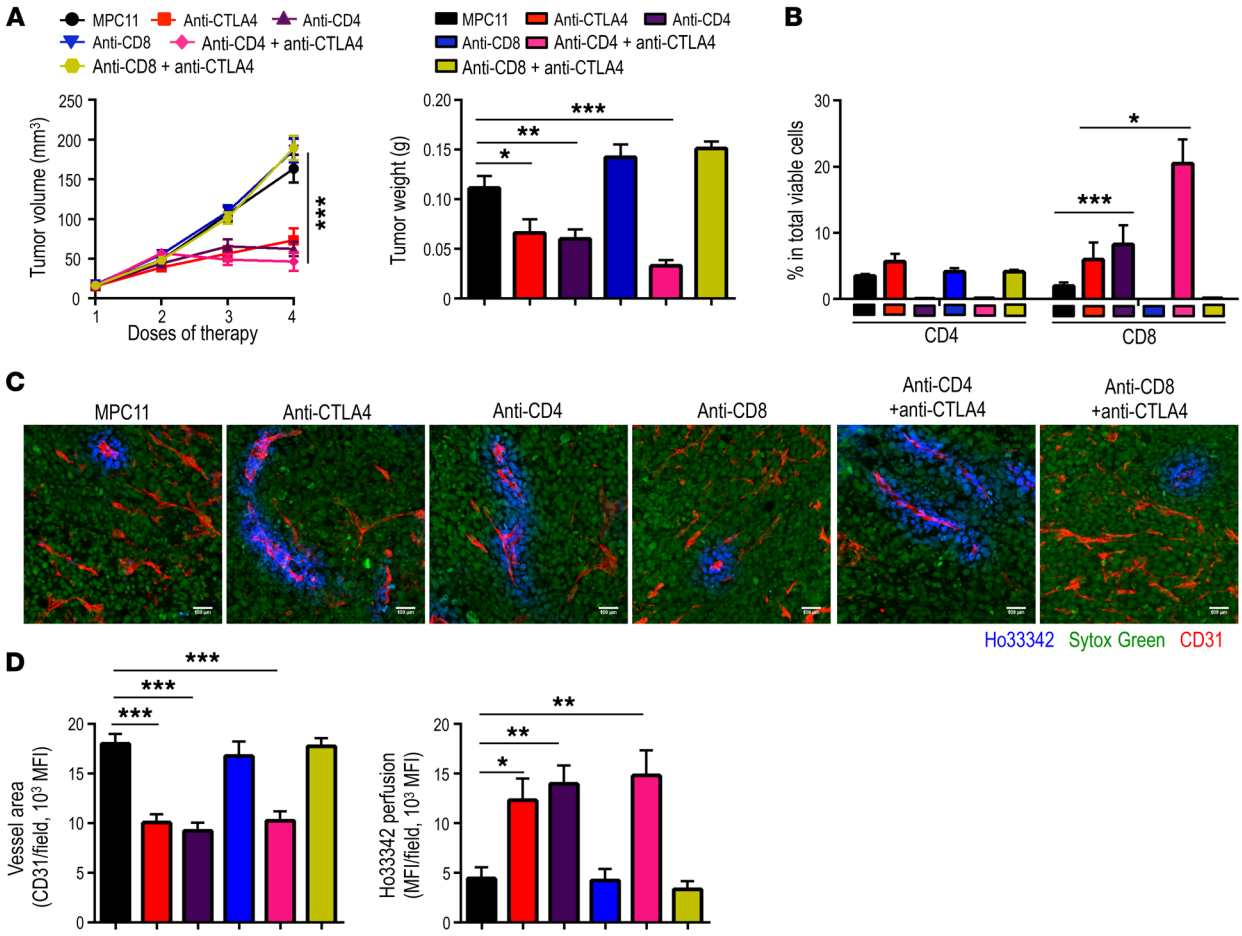

Figure 5. CD8⁺ T cells mediate the effects of anti–CTLA4 therapy on tumor growth and vessel perfusion. EO771 tumor preparation, anti–CD8, or anti–CD4 antibody administrations were done as described for Figure 4. (**A**) In vivo depletion of CD8⁺ T cells, but not CD4⁺ T cells, abolished the antitumor effect of anti–CTLA4 therapy as compared with the control group. (**B**) CD8⁺ T cell depletion did not affect CD4⁺ T cell tumor accumulation, but CD4⁺ T cell depletion increased CD8⁺ T cell tumor accumulation. (**C** and **D**) CD8⁺, but not CD4⁺, T cell depletion completely reversed the effect of anti–CTLA4 therapy on tumor vessel perfusion. Scale bars: 100 μM. Significance was determined by 1-way ANOVA with Bonferroni's adjusted post hoc *t* tests for multiple comparisons. Data are from 1 experiment representative of 2 independent experiments (n = 8–10 mice per group). $^*P < 0.05$, $^{**}P < 0.01$, $^{***}P < 0.001$.

Prospective detection of global enhancement in tumor vessel perfusion predicts therapeutic outcomes of anti–CTLA4 therapy. To test the translational possibility that monitoring IVP can prospectively identify tumor-bearing hosts who will respond to ICB, we measured overall changes in tumor vessel perfusion after treatment with ICB by using a clinically relevant imaging strategy. Here, we adapted 3D ultrasonography and color Doppler measurement to estimate tumor volume and the percentage of perfused tumor vessel volume, respectively (Figure 9A). We first measured the percentage of perfused tumor vessel volume on day 6 after anti–CTLA4 treatment in EO771 breast tumors. We then divided the tumors into perfusion-high and perfusion-low groups based on the mean percentage of perfused vessel volume (6.46%) as a cutoff. Global tumor vessel perfusion was found to be significantly increased by anti–CTLA4 therapy in the perfusion-high group as compared with MPC11 control and perfusion-low groups (Figure 9, A and B). We then monitored tumor growth until day 12 to identify responders and nonresponders to anti–CTLA4 therapy. Four out of 5 perfusion-high tumors were identified as ICB responders on day 12, whereas no perfusion-low tumors were ICB responders, corresponding to more than 90% sensitivity and specificity (Figure 9, B and C). These findings suggest that global changes in tumor vessel perfusion by ICB can be measured noninvasively by radiological methods to predict individual responses to ICB therapy.

Discussion

Conventional chemotherapy acts by killing proliferating cells, and it has antitumor effects in most patients with cancer. However, its overall effectiveness is marginal and transient. Unlike chemotherapy, ICB exerts its antitumor effect by resuscitating the host immune system, and thus the response is theoretically durable and potentially even curative.

ICB represents a new cancer treatment modality with several unique characteristics (2, 3, 6). First, ICB has long-term survival benefits in only a small fraction of patients. Second, ICB often has an uncertain latent period before its effectiveness in a patient can be determined. Third, ICB can elicit inflammatory responses in nontumor sites, which can cause serious side effects. These features, in addition to its high cost, have prompted numerous efforts to identify reliable biomarkers in ICB (2, 3, 6). In this study, we

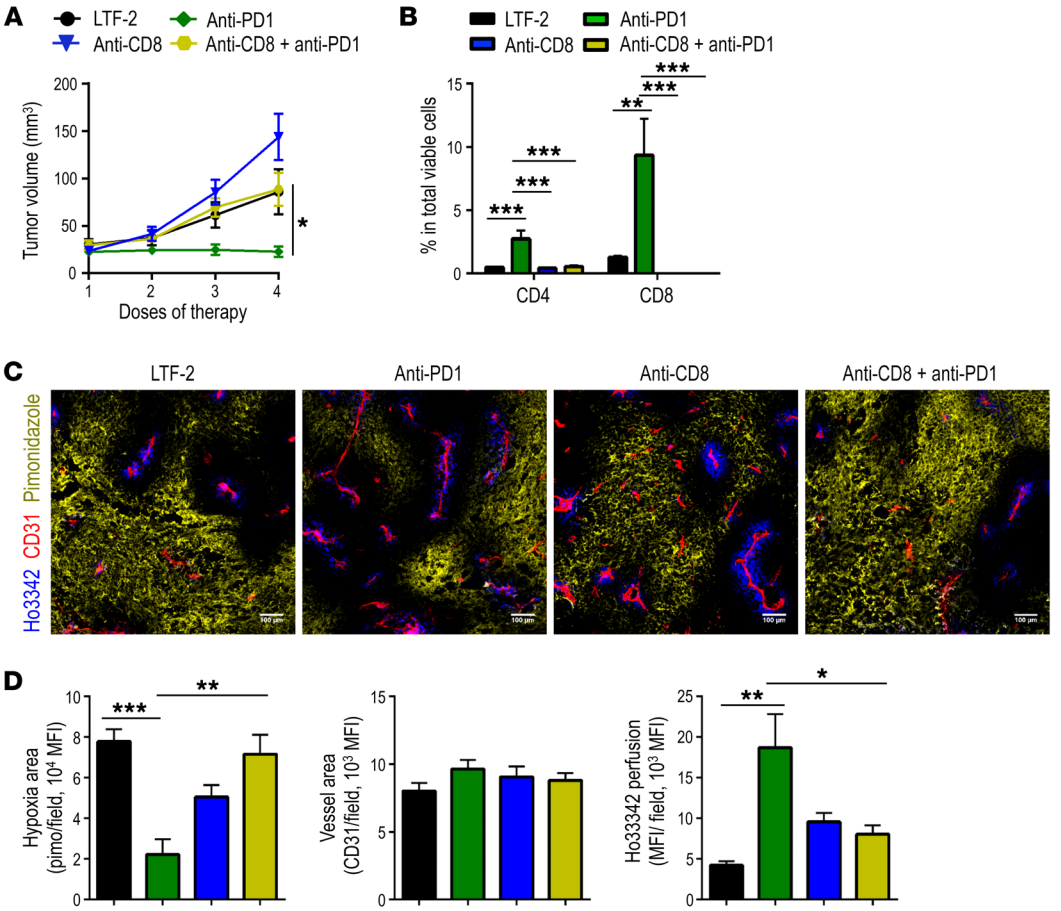

Figure 6. Anti–PD1 therapy inhibits tumor growth and improves vessel perfusion via CD8⁺ T cells. When MCA38 colon tumors reached 4–6 mm in diameter, mice were randomly assigned to 4 groups and treated with isotype IgG (LTF2), an anti–PD1 antibody (10 mg/kg), an anti–CD8 antibody, or the combination for 4 doses every 3 days. (**A**) In vivo depletion of CD8⁺ T cells abrogated the antitumor effect of anti–PD1 therapy. (**B**) CD8⁺ T cell depletion did not affect CD4⁺ T cell tumor infiltration. (**C** and **D**) CD8⁺ T cell depletion abrogated the effects of anti–PD1 therapy on tumor tissue hypoxia and vessel perfusion. Scale bars: 100 μM. Significance was determined by 1-way ANOVA with Bonferroni's adjusted post hoc *t* tests for multiple comparisons. Data are from 1 experiment representative of 2 independent experiments (n = 8–10 mice per group). $^*P < 0.05$, $^{**}P < 0.01$, $^{***}P < 0.001$.

showed that the ability of ICB to increase tumor vessel perfusion could distinguish sensitive from resistant tumors in mouse models of breast cancer. In one sensitive tumor model, the extent of ICB-induced IVP correlated with the antitumor effect. To our knowledge, this is the first study to suggest that measurements of vessel perfusion could be used to predict the ICB efficacy.

Compared with blood vessels in normal tissues, tumor vessels are chaotic and their functional capacity is disrupted. These aberrancies in tumor vasculature result in a hypoxic TME, which is known to contribute to various kinds of immunosuppression, thereby impeding cancer immunotherapies (21, 22, 31–33). Hypoxia in tumor tissue induces the expression of ectoenzymes, such as CD73, leading to the accumulation of extracellular adenosine. Subsequently, adenosine interacts with its receptors A2A and A2B to produce immunosuppressive factors and suppress immune effector cell activation (34–38). We found that CD73 is highly expressed in ICB-resistant 4T1 and MCaP0008 tumor cells (Supplemental Figure 11). Moreover, respiratory hyperoxia (60% oxygen) has been shown to reverse hypoxia-adenosine–mediated immunosuppression and to induce tumor regression in a T cell– and natural killer cell–dependent manner (39, 40). Additionally, targeting proangiogenic factors could improve vessel perfusion and alleviate immunosuppression in the TME, improving therapeutic efficacy in preclinical studies (16, 21, 22). In theory then, ICB-mediated increases in vessel perfusion and decreases in TME hypoxia in a given tumor would convert the TME from immunosuppressive to immunopermissive. Such changes to the TME may facilitate tumor infiltration of CD8⁺ T cells and increase the production of proinflammatory cytokines including IFN-γ, which in turn would sustain ICB-activated T effector cells. Such a positive feedback loop from immune-vascular crosstalk would reinforce ICB-induced antitumor immunity, leading to eventual cancer eradication (23). Conversely, if ICB fails to enhance tumor vessel function, the immunosuppressive TME may compromise the function of ICB-activated T cells, resulting in poor therapeutic outcomes. From this point of view, IVP may be a prerequisite for ICB to convert a given tumor from immune-evading status into a form that could be eliminated by the immune system.

In this study, we provided several lines of evidence to support IVP as a novel indicator for predicting ICB responsiveness.

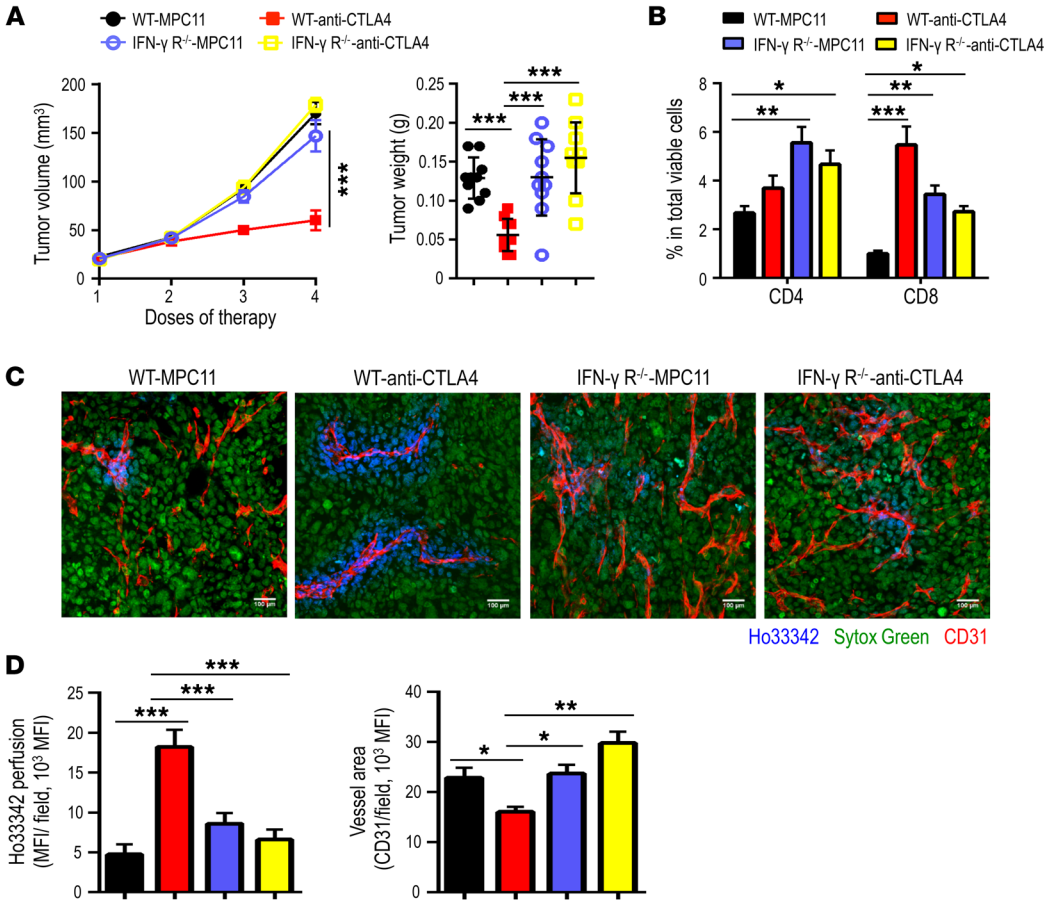

Figure 7. IFN-γ receptor deficiency negates the effects of anti–CTLA4 therapy on tumor growth and vessel perfusion. EO771 tumor cells were inoculated orthotopically in WT and IFN-γR$^{-/-}$ mice. When tumors reached 3–4 mm in diameter, mice were randomly assigned to 2 groups and treated with an anti–CTLA4 antibody or MPC11 (5 mg/kg) every 3 days for a total of 4 doses. (**A**) Anti–CTLA4 therapy lost its antitumor effect in IFN-γR$^{-/-}$ mice, compared with WT mice. (**B**) IFN-γ receptor deficiency partially reversed the increase of CD8$^+$ T cells upon anti–CTLA4 therapy. (**C** and **D**) IFN-γ receptor deficiency completely reversed IVP induced by anti–CTLA4 therapy. Scale bars: 100 μM. Significance was determined by 1-way ANOVA with Bonferroni's adjusted post hoc *t* tests for multiple comparisons (n = 10 mice per group). *P < 0.05, **P < 0.01, ***P < 0.001.

First, IVP could efficiently identify ICB responsive tumors. In our study, IVP was observed only in ICB-sensitive tumor models, and the increased levels of vessel perfusion positively correlated with the effectiveness of the ICB. Second, IVP reflects the overall ability of ICB to stimulate antitumor T cell immunity and to sustain the activity of T cells to eradicate cancer cells. We showed that ICB increased vessel perfusion in responsive tumors by increasing CD8$^+$ T cell number and IFN-γ production. The ability of ICB to stimulate CD8$^+$ T cells to produce adequate IFN-γ to remodel tumor vessels indicates that ICB is sufficient to overcome the overall immunosuppression in responsive tumors. Importantly, noninvasive ultrasound scanning could detect ICB-induced global changes in tumor vessel perfusion before changes in tumor size became evident, and the extent of those changes predicted the therapeutic effectiveness of the ICB agent (Figure 9). Thus, IVP has an advantage compared with current biomarkers that are mainly derived from tumor tissue samples. In the clinic, radiologic methods have been used to evaluate tumor vessel perfusion in the context of antiangiogenic treatment (41, 42). Similar noninvasive methods can be used to measure IVP as a novel TME-based indicator to predict ICB effectiveness in real time (23).

Immune cell responses in general, and T cell activation in particular, have been used to evaluate the effectiveness of ICB in both preclinical and clinical studies to date. However, because of the immunosuppressive characteristics of the TME, peripheral immune cells often do not reflect the actual status of immune cells within the TME and often fail to predict the effectiveness of ICB for individual patients. In our study, ICB-induced vascular responses, and IVP in particular, were observed in all of the responding tumors. Thus, vessel perfusion could be used to distinguish responders from nonresponders in the early stages of this expensive and potentially toxic treatment (Supplemental Figure 12). Given that vascular perfusion can be monitored in real time by noninvasive radiologic methods, it is conceivable that IVP could substantially upgrade the current practice of cancer immunotherapy to achieve genuinely personalized cancer immunotherapies to benefit patients with cancer.

Methods

Tumor models. FVB mice (an inbred mouse strain named for its susceptibility to Friend leukemia virus B) were bred and maintained in a gnotobiotic animal facility at Soochow University. C56BL/6 and Balb/c mice were from commercial vendors. IFN-γR$^{-/-}$ mice congenic to

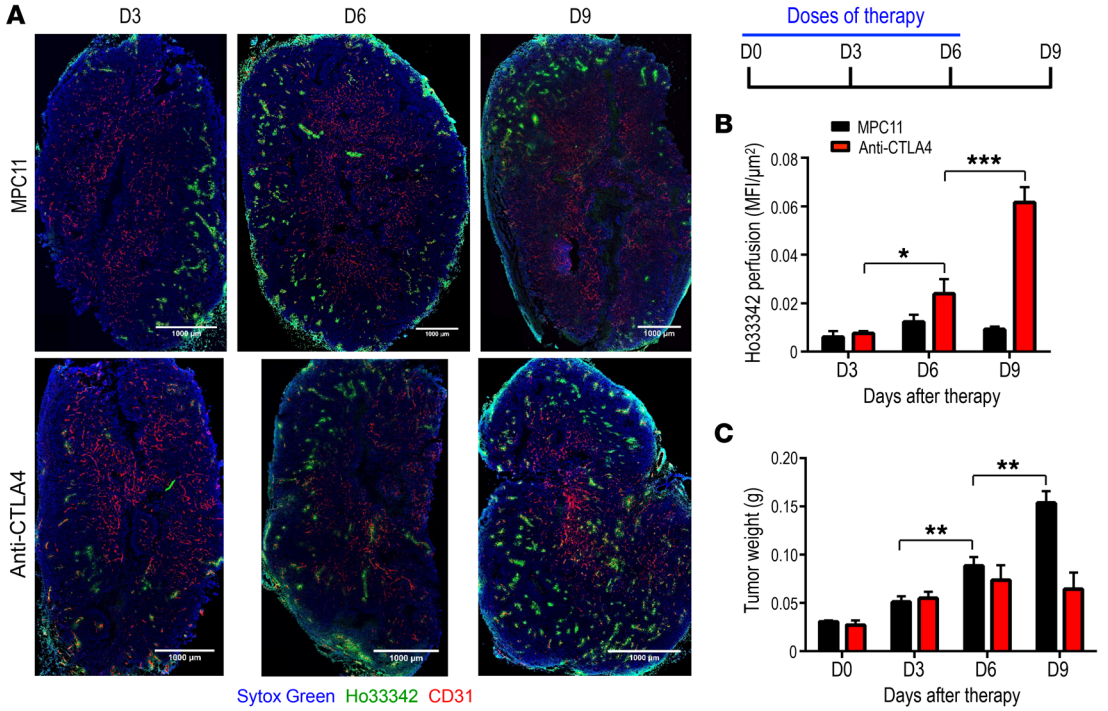

Figure 8. Anti–CTLA4 therapy increases vessel perfusion in a time-dependent manner before tumor size changes are detectable. When EO771 breast tumors reached 3–4 mm in diameter, mice were randomly assigned to 1 of 6 groups and treated on day 0 with an anti–CTLA4 antibody or MPC11 (5 mg/kg) every 3 days. Tumor tissues were isolated on days 3, 6, or 9 after anti–CTLA4 treatment. Vessel perfusion over the entire cross section of tumor tissues was assessed by confocal microscopy. (**A**) Representative whole-tumor tissue perfusion images. Scale bars: 1,000 μM. (**B**) Vessel perfusion was significantly increased in a time-dependent manner in the anti-CTLA4–treated group. (**C**) Tumor weight did not significantly change between days 3, 6, and 9 in the anti-CTLA4–treated group. Ho33342 (green), Hoechst 33342 perfused area; CD31 (red), endothelial cells; and Sytox Green (blue), counterstained for tumor tissue. Significance was determined by unpaired 2-tailed Student's *t* tests. Data are from 1 experiment representative of 2 independent experiments. Each group had 5–6 mice on days 3 and 6, or 5–9 mice on day 9. $^{*}P < 0.05$, $^{**}P < 0.01$, $^{***}P < 0.001$.

C57BL/6 were originally from Jackson Laboratories and maintained by Zhihai Qin at the Institute of Biophysics, Chinese Academy of Sciences (Beijing, China) (43). Female mice (6–8 weeks old) were used in all the studies. Fragments (1–2 mm^3) of spontaneous MMTV-PyVT breast cancers were orthotopically transplanted into syngeneic FVB female mice for less than 5 generations. The EO771 breast tumor cell line was purchased from CH3 Biosystems. The 4T1, MCA38, and CT26 tumor cell lines were purchased from American Type Culture Collection. The MCaP0008 breast tumor cell line was generated by Peigen Huang at Massachusetts General Hospital (Boston, Massachusetts, USA) (44). The 4T1 cells were cultured with RPMI-1640 containing 10% fetal bovine serum; all other cell lines were cultured with DMEM and 10% fetal bovine serum. Cell cultures were frequently monitored for mycoplasma contamination, and only mycoplasma-negative cells were used for experiments. MCaP0008, 4T1, and EO771 mammary carcinoma cells (2×10^5 cells) were injected orthotopically into the third mammary fat pad of female FVB, Balb/c, and C57BL/6 mice, respectively. MCA38 and CT26 colon carcinoma cells (3×10^5 cells) were inoculated subcutaneously into the right flank of C56BL/6 and Balb/c mice, respectively. When tumors reached 3–6 mm in diameter, mice were randomly assigned to treatment groups and received i.p. injection of either isotype-matched control IgG_{2b} (catalog BE0086, clone MPC11, 5 mg/kg), IgG_{2a} (catalog BE0089, clone 2A3, 5 mg/kg), rat IgG_1 (catalog BE0088, clone HRPN, 250 μg/mouse), anti–CTLA4 (catalog BE0164, clone 9D9, 5 mg/kg), anti–PD1 (catalog BE0273, clone 29F.1A12, 10 mg/kg), or anti–IFN-γ (catalog BE0055, clone XMG1.2, 250 μg/mouse) antibodies (all from Bio-X Cell). Antibody treatments and tumor measurements were conducted every 3 days. When mice were euthanized, the tumors were removed and weighed. The sample size for the mouse studies was determined based on estimates from pilot experiments and previous experience to ensure that appropriate statistical tests could yield significant results. Mice were randomly assigned to appropriate groups to ensure that all groups began treatment with tumors of similar sizes.

Tumor vessel perfusion analysis. Tumor tissue perfusion was evaluated by histologic analysis of the intravenously injected perfusion marker Hoechst 33342 (Sigma-Aldrich), based on our previously published method (16). Briefly, 5 minutes after i.v. injection of Hoechst 33342 (10 mg/kg in 200 μL PBS) mice were systemically perfused with PBS, and the tumors were removed and fixed with 4% paraformaldehyde. This procedure stained the perfused vessels with fluorescent nucleus-bound Hoechst 33342. Mosaic images of tumors were collected with an Olympus FV1000 confocal laser-scanning microscope. A ×20 objective was used to acquire 640 × 640 μm tiles, and an automated stage was used to scan through the entire cross section of tumor tissues. The imaged tiles were stitched into a final mosaic image by using Olympus software. Nonspecific nuclear staining (Sytox Green, Molecular Probes) was used to counterstain the slides. In each field, the mean fluorescence intensity of both $CD31^+$ and Hoechst 33342^+ areas was calculated by using Image-Pro plus software (version 6.0).

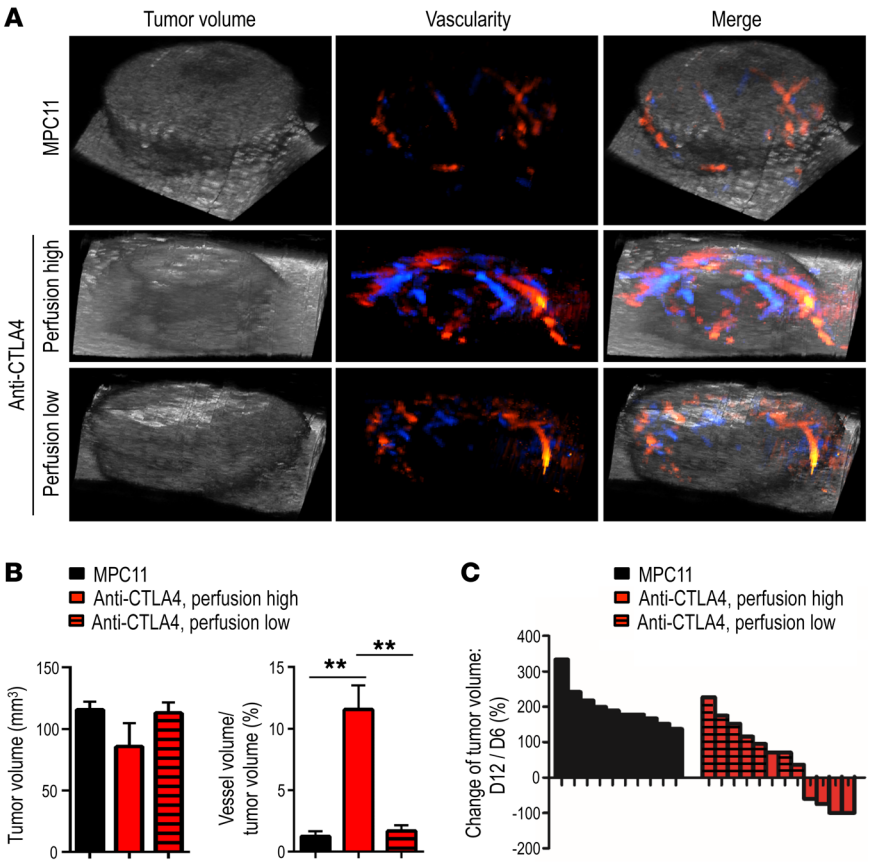

Figure 9. A global increase in tumor vessel perfusion on sonography on day 6 predicts the responsiveness to anti–CTLA4 therapy. EO771 tumors were prepared and treated as described in Figure 8. EO771 breast tumors were scanned by ultrasonography on day 6 after anti–CTLA4 therapy. (**A**) Representative 3D images of tumor volume and vascularity on day 6. The blue and red colors represent different blood flow directions. (**B**) Anti–CTLA4 therapy increased vessel perfusion in perfusion-high tumors as compared with perfusion-low tumors or the control group, but tumor volume did not differ among the 3 groups on day 6. EO771 tumors treated with anti–CTLA4 therapy were stratified as perfusion high (5 tumors) or perfusion low (7 tumors) according to the mean value of the percentage of perfused vessel volume measured on day 6. (**C**) Four of 5 perfusion-high tumors were identified as responders on day 12 after 4 cycles of anti–CTLA4 therapy, whereas all of the perfusion-low tumors were nonresponders (n = 10–12 mice per group). Significance was determined by unpaired 2-tailed Student's t tests. $^{**}P < 0.01$.

Pimonidazole staining. For hypoxia studies, pimonidazole (15 mg/kg in 100 μL saline, Hypoxyprobe) was injected intravenously and left to circulate for 25 minutes. Then mice were systemically perfused with PBS, and the tumors were removed and immediately frozen in liquid nitrogen. Tumor sections were stained with a Hypoxyprobe Plus Kit according to the manufacturer's protocol (catalog HP8-100Kit).

Immunohistochemical staining. Tumor tissues were fixed in 4% paraformaldehyde for 2 to 3 hours, followed by incubation in 30% sucrose overnight at 4°C. The tissues were OCT-embedded and kept at –80°C. Staining for the endothelial marker CD31 (1:100, clone MEC13.3, catalog 550274, BD Biosciences) and the pericyte marker NG2 (1:1,000, clone 7B12.2, catalog MAB5320, Chemicon) was done on frozen sections (20-μm thickness), followed by staining with secondary antibody Alexa Fluor 647 donkey anti–rat IgG (catalog 712-605-153) and Cy3-donkey anti-rabbit (catalog 711-165-152) (1:200, both from Jackson ImmunoResearch) in dark, humid chambers at room temperature. The slides were counterstained for cell nuclei by Sytox Green or 4,6-diamidino-2-phenylindole. Fluorescent images were obtained with an Olympus FV1000 confocal laser-scanning microscope. Microvessel density and pericyte coverage were assessed by using ImagePro plus software (version 6.0). The variables were determined for 4–6 photographic areas from each tumor (640 × 640 μm^2 each). Confocal images were taken in randomly selected fields, excluding the tumor periphery (4–6 fields per tumor).

Survival analysis. EO771 mammary carcinoma cells (2 × 10^5 cells) were inoculated orthotopically into female C57BL/6 mice. When tumors reached 3–4 mm in diameter, mice were randomly assigned to 1 of 2 groups and given i.p. injection of either control MPC11(5 mg/kg) or anti–CTLA4 antibody (5 mg/kg) every 3 days for a total of 5 doses. Tumor size was measured every 3 days for 60 days. Mice were euthanized when the estimated tumor volumes reached 1,000 mm^3. The following formula was used to estimate tumor volume (mm^3) = (long axis) × (short axis)^2 × π/6. Survival curves for mice given anti–CTLA4 therapy were analyzed by the Kaplan-Meier method. Mice with completely regressed tumors were rechallenged with 2 × 10^5 EO771 cancer cells on the opposite site of the third mammary fat pad, and tumor growth was monitored for another 3 weeks. Naive mice that received the same number of EO771 cancer cells were used as controls.

Color Doppler angiography of tumor blood vessels. Murine ultrasonographic imaging was done as previously described, with modifications (45, 46). Briefly, breast tumors were visualized by using a Vevo 2100 Imaging System with 550D scan probe (VisualSonics Inc.) at 32 MHz. EO771 tumor-bearing mice were anesthetized with 2% isoflurane (RWD Life Science) and hair around the tumor area was removed with a pet trimmer (Codos, CP-3800). Mice were placed supine on a warmed platform to maintain body temperature and record heart rate. The ultrasound probe was covered with a large amount of ultrasonic coupling agent to avoid any effects of external pressure on tumor blood flow. The 3D mode was used to collect data in x, y, and z directions. Step size was set at 0.1 mm for each 3D scan. Perfused tumor blood vessel volume was recorded by the 3D imaging motor in the color Doppler mode. The percentage of tumor blood volume in tumor tissues was analyzed according to the manufacturer's instructions. Tumor-bearing mice were monitored after imaging for 6 days to identify responders and nonresponders to anti–CTLA4 therapy.

T cell depletion and IFN-γ blockade. $CD4^+$ and $CD8^+$ T cells were depleted according to a published method (16). Briefly, EO771 tumor-bearing mice were given i.p. injections of 200 μg isotype-matched control IgG_{2b} (catalog BE0090, clone LTF-2, Bio-X Cell), anti–CD4 monoclonal antibody (catalog BE0003, clone GK1.5, Bio-X Cell), and/or 200 μg anti–CD8 monoclonal antibody (catalog BE0004, clone 53-6.72, Bio-X Cell) or 2A3, on days 0, 2, and 8. At the end of the experiment, the efficiency of $CD4^+$ and $CD8^+$ T cell depletion was verified by flow cytometry. For IFN-γ neutralization, EO771 tumor-bearing mice were given i.p. injections of 250 μg anti–IFN-γ antibody (catalog BE0055, clone XMG1.2, Bio-X Cell) or rat IgG1 on days 0, 3, 6, and 9.

Flow cytometric analysis. Tumor-bearing mice were euthanized and immediately given an intracardiac injection of PBS, after which tumor tissues were isolated, minced, and digested at 37°C for 45 minutes with DMEM containing collagenase type 1A (1.5 mg/ml), hyaluronidase (1.5 mg/ml), and DNase (20 U/ml). The digested mixtures were filtered through 70-μm cell strainers. Single-cell suspensions were incubated with a rat anti–mouse CD16/CD32 monoclonal antibody (catalog 553142, clone 2.4G2, BD Pharmingen), and then stained, washed, and resuspended in cold flow buffer (1% bovine serum albumin, 0.1% NaN_3 in PBS). The following fluorochrome-conjugated antibodies were used: CD45-PE-Cy7 (catalog 552848, clone 30-F11), CD45-BV421 (catalog 563890, clone 30-F11), CD11b-BV510 (catalog 562950, clone M1/70), CD11b-APC-Cy7 (catalog 557657, clone M1/70), CD4-PE (catalog 553730, clone RM4-5), CD8-FITC (catalog 553031, clone 53-6.7), Ly-6G-FITC (catalog 551460, clone 1A8), Ly-6C-PE (catalog 560592, clone AL-21), Gr-1–APC-Cy7 (catalog 557661, clone RB6-8C5), IFN-γ–PE-Cy7 (catalog 557649, clone XMG1.2), and CD73–Alexa Fluor 647 (catalog 561543, clone TY/23) (all from BD Pharmingen); and F4/80-FITC (catalog 123108, clone BM8) and F4/80-APC (catalog 123116, clone BM8) (BioLegend). The reagent 7-amino-actinomycin D (7AAD, eBioscience) was added to the stained samples (5 μL/tube) just before flow cytometric analysis. The doublet/aggregated events were gated out using side scatter area versus side scatter width. For intracellular IFN-γ staining, 2×10^6 cells were cultured with 700 μl RPMI-1640 medium containing 10% fetal bovine serum and 0.1% Brefeldin A solution (catalog 420601, eBioscience) in a 24-well plate for 4 hours. Cells were then collected for extracellular staining, followed by intracellular staining using a Fixation/Permeabilization Solution Kit (catalog 554714, BD Bioscience) according to the manufacturer's instructions. IFN-γ–expressing T cells were determined and quantified through fluorescence-minus-one gating strategy. All of the samples were analyzed on a Gallios flow cytometer (Beckman), and data were analyzed with Kaluza software (version 1.3).

Quantitative real-time PCR. Total RNA from tumor tissues or separated cells was isolated with a MicroElute Total RNA kit (Omega), followed by cDNA synthesis with a RevertAid First Strand cDNA Synthesis Kit (ThermoFisher Scientific). Gene expression was assessed by qPCR with Light Cycler 480 SYBR Green I Master mix and primers (Supplemental Table 1) in a High Throughput Quantitative PCR Light Cycler480 (Roche). To avoid nonspecific amplification, primers were designed so that one half hybridized to the 3′ end of one exon, and the other half hybridized to the 5′ end of the adjacent exon. The comparative threshold cycle method was used to calculate differences in gene expression (fold change), which was normalized to *B-actin* as the reference gene.

Statistics. Statistical analyses were done with Prism software (version 6, GraphPad). All comparisons between 2 groups were made with unpaired 2-tailed Student's *t* tests. When more than 2 groups were assessed, after confirmation that normality was achieved (using the Kolmogorov-Smirnov test in PRISM), data were assessed by 1-way ANOVA followed by Bonferroni's adjusted post hoc *t* tests for multiple pairs of interest without a priori selection. Log-rank tests were used to compare survival data. Robust regression and outlier removal (ROUT, GraphPad) were used to determine whether outliers were present. Experiments were typically repeated at least 3 times, unless otherwise noted. Data are presented as mean ± SEM. All statistical tests were 2-sided, and results were considered statistically significant at $P < 0.05$.

Study approval. Animal studies with IFN-$\gamma R^{-/-}$ mice were conducted under protocols approved by the institutional animal care and use committee of the Institute of Biophysics, Chinese Academy of Sciences (Beijing, China). All the other animal studies were approved by the institutional animal care and use committee of Soochow University. Mice were kept in a specific pathogen–free facility in microisolator cages. All experimental methods were conducted in accordance with the animal care and use regulations of China.

Author contributions

YH conceived and supervised the study. XZ, ZF, XXW, XL, SD, PZ, CZ, RY, HH, XC, and YJH performed the experiments and analyzed the data. SQ, XHW, YZ, SL, PHZ, BYSK, WJ, and QW interpreted the data and provided intellectual input. XZ, ZF, WJ, and YH designed the experiments, analyzed the data, and interpreted the results. YH wrote and revised the manuscript with XZ, BYSK, WJ, QW, and with input from other authors.

Acknowledgments

We are grateful to Rakesh K. Jain (Harvard Medical School), Yufang Shi (Soochow University), Suling Liu (University of Science and Technology of China), Zhihai Qin (Institute of Biophysics, Chinese Academy of Sciences), Zhinan Yin (Jinan University), Yuting Ma (Suzhou Institute of Systems Medicine, Chinese Academy of Medical Sciences), Xiaoren Zhang (Suzhou Institute of Systems Medicine, Chinese Academy of Medical Sciences), and Youfa Duan (Sun Yat-Sen University Cancer Center) for technical support and expert advice. This work was supported in part by the National Natural Science Foundation of China grants 81673004 and 81372245 (to YH), the National Program on Key Research Project of China 2016YFC1302400 (to YH), the Distinguished Professors of Jiangsu Province fund SR21100114 (to YH), the Collaborative Innovation Center of Hematology, the Priority Academic Program Development of Jiangsu Higher Education Institutions, the National Institute of Neurological Disorders and Stroke grant R01 NS104315 (to BYSK), the American Society of Clinical Oncology Conquer Cancer Foundation Young Investigator Award (to WJ), and the National Cancer Institute's Cancer Center Support (Core) grant CA016672 (to the University of Texas MD Anderson Cancer Center). The authors also thank C. Wogan of the MD Anderson Cancer Center's Division of Radiation Oncology for editorial assistance.

Address correspondence to: Yuhui Huang, Cyrus Tang Hematology Center, Soochow University, 199 Ren-Ai Road, Suzhou 215123, Jiangsu, China. Phone: 0086.512.65880877; Email: hyhui20126@163.com or huangyh@suda.edu.cn.

1. Chen L, Han X. Anti-PD-1/PD-L1 therapy of human cancer: past, present, and future. *J Clin Invest*. 2015;125(9):3384–3391.
2. Sharma P, Allison JP. The future of immune checkpoint therapy. *Science*. 2015;348(6230):56–61.
3. Topalian SL, Taube JM, Anders RA, Pardoll DM. Mechanism-driven biomarkers to guide immune checkpoint blockade in cancer therapy. *Nat Rev Cancer*. 2016;16(5):275–287.
4. Nishino M, Ramaiya NH, Hatabu H, Hodi FS. Monitoring immune-checkpoint blockade: response evaluation and biomarker development. *Nat Rev Clin Oncol*. 2017;14(11):655–668.
5. Chen L, Flies DB. Molecular mechanisms of T cell co-stimulation and co-inhibition. *Nat Rev Immunol*. 2013;13(4):227–242.
6. Zou W, Wolchok JD, Chen L. PD-L1 (B7-H1) and PD-1 pathway blockade for cancer therapy: mechanisms, response biomarkers, and combinations. *Sci Transl Med*. 2016;8(328):328rv4.
7. Hodi FS, et al. Immunologic and clinical effects of antibody blockade of cytotoxic T lymphocyte-associated antigen 4 in previously vaccinated cancer patients. *Proc Natl Acad Sci U S A*. 2008;105(8):3005–3010.
8. Brahmer JR, et al. Phase I study of single-agent anti-programmed death-1 (MDX-1106) in refractory solid tumors: safety, clinical activity, pharmacodynamics, and immunologic correlates. *J Clin Oncol*. 2010;28(19):3167–3175.
9. Topalian SL, et al. Safety, activity, and immune correlates of anti-PD-1 antibody in cancer. *N Engl J Med*. 2012;366(26):2443–2454.
10. Fusi A, et al. PD-L1 expression as a potential predictive biomarker. *Lancet Oncol*. 2015;16(13):1285–1287.
11. Van Allen EM, et al. Genomic correlates of response to CTLA-4 blockade in metastatic melanoma. *Science*. 2015;350(6257):207–211.
12. Rizvi NA, et al. Cancer immunology. Mutational landscape determines sensitivity to PD-1 blockade in non-small cell lung cancer. *Science*. 2015;348(6230):124–128.
13. Atrash S, Makhoul I, Mizell JS, Hutchins L, Mahmoud F. Response of metastatic mucosal melanoma to immunotherapy: it can get worse before it gets better. *J Oncol Pharm Pract*. 2017;23(3):215–219.
14. Hodi FS, et al. Evaluation of immune-related response criteria and RECIST v1.1 in patients with advanced melanoma treated with pembrolizumab. *J Clin Oncol*. 2016;34(13):1510–1517.
15. Demaria S, et al. Immune-mediated inhibition of metastases after treatment with local radiation and CTLA-4 blockade in a mouse model of breast cancer. *Clin Cancer Res*. 2005;11(2 pt 1):728–734.
16. Huang Y, et al. Vascular normalizing doses of antiangiogenic treatment reprogram the immunosuppressive tumor microenvironment and enhance immunotherapy. *Proc Natl Acad Sci U S A*. 2012;109(43):17561–17566.
17. Holmgaard RB, Zamarin D, Munn DH, Wolchok JD, Allison JP. Indoleamine 2,3-dioxygenase is a critical resistance mechanism in antitumor T cell immunotherapy targeting CTLA-4. *J Exp Med*. 2013;210(7):1389–1402.
18. Grosso JF, Jure-Kunkel MN. CTLA-4 blockade in tumor models: an overview of preclinical and translational research. *Cancer Immun*. 2013;13:5.
19. Tian L, et al. Mutual regulation of tumour vessel normalization and immunostimulatory reprogramming. *Nature*. 2017;544(7649):250–254.
20. Jain RK. Antiangiogenesis strategies revisited: from starving tumors to alleviating hypoxia. *Cancer Cell*. 2014;26(5):605–622.
21. Hamzah J, et al. Vascular normalization in Rgs5-deficient tumours promotes immune destruction. *Nature*. 2008;453(7193):410–414.
22. Johansson A, Hamzah J, Payne CJ, Ganss R. Tumor-targeted TNFα stabilizes tumor vessels and enhances active immunotherapy. *Proc Natl Acad Sci U S A*. 2012;109(20):7841–7846.
23. Huang Y, Kim BYS, Chan CK, Hahn SM, Weissman IL, Jiang W. Improving immune-vascular crosstalk for cancer immunotherapy. *Nat Rev Immunol*. 2018;18(3):195–203.
24. Jain RK. Normalization of tumor vasculature: an emerging concept in antiangiogenic therapy. *Science*. 2005;307(5706):58–62.
25. Huang Y, Stylianopoulos T, Duda DG, Fukumura D, Jain RK. Benefits of vascular normalization are dose and time dependent — letter. *Cancer Res*. 2013;73(23):7144–7146.
26. Hodi FS, et al. Improved survival with ipilimumab in patients with metastatic melanoma. *N Engl J Med*. 2010;363(8):711–723.
27. Shankaran V, et al. IFNgamma and lymphocytes prevent primary tumour development and shape tumour immunogenicity. *Nature*. 2001;410(6832):1107–1111.
28. Meunier MC, Delisle JS, Bergeron J, Rineau V, Baron C, Perreault C. T cells targeted against a single minor histocompatibility antigen can cure solid tumors. *Nat Med*. 2005;11(11):1222–1229.
29. Rüegg C, Yilmaz A, Bieler G, Bamat J, Chaubert P, Lejeune FJ. Evidence for the involvement of endothelial cell integrin alphaVbeta3 in the disruption of the tumor vasculature induced by TNF and IFN-gamma. *Nat Med*. 1998;4(4):408–414.
30. Benci JL, et al. Tumor interferon signaling regulates a multigenic resistance program to immune checkpoint blockade. *Cell*. 2016;167(6):1540–1554.e12.
31. Huang Y, Goel S, Duda DG, Fukumura D, Jain RK. Vascular normalization as an emerging strategy to enhance cancer immunotherapy. *Cancer Res*. 2013;73(10):2943–2948.
32. Palazón A, Aragonés J, Morales-Kastresana A, de Landázuri MO, Melero I. Molecular pathways: hypoxia response in immune cells fighting or promoting cancer. *Clin Cancer Res*. 2012;18(5):1207–1213.
33. Noman MZ, et al. PD-L1 is a novel direct target of HIF-1α, and its blockade under hypoxia enhanced MDSC-mediated T cell activation. *J Exp Med*. 2014;211(5):781–790.
34. Ohta A, et al. A2A adenosine receptor protects tumors from antitumor T cells. *Proc Natl Acad Sci U S A*. 2006;103(35):13132–13137.
35. Sitkovsky MV, Hatfield S, Abbott R, Belikoff B, Lukashev D, Ohta A. Hostile, hypoxia-A2-adenosinergic tumor biology as the next barrier to overcome for tumor immunologists. *Cancer Immunol Res*. 2014;2(7):598–605.
36. Sitkovsky MV. T regulatory cells: hypoxia-adenosinergic suppression and re-direction of the immune response. *Trends Immunol*. 2009;30(3):102–108.
37. Loi S, et al. CD73 promotes anthracycline resistance and poor prognosis in triple negative breast cancer. *Proc Natl Acad Sci U S A*. 2013;110(27):11091–11096.
38. Beavis PA, et al. Blockade of A2A receptors potently suppresses the metastasis of CD73+ tumors. *Proc Natl Acad Sci U S A*. 2013;110(36):14711–14716.
39. Hatfield SM, et al. Immunological mechanisms of the antitumor effects of supplemental oxygenation. *Sci Transl Med*. 2015;7(277):277ra30.
40. Hatfield SM, et al. Systemic oxygenation weakens the hypoxia and hypoxia inducible factor 1α-dependent and extracellular adenosine-mediated tumor protection. *J Mol Med*. 2014;92(12):1283–1292.
41. Batchelor TT, et al. Improved tumor oxygenation and survival in glioblastoma patients who show increased blood perfusion after cediranib and chemoradiation. *Proc Natl Acad Sci U S A*. 2013;110(47):19059–19064.
42. Emblem KE, et al. Vessel architectural imaging identifies cancer patient responders to anti-angiogenic therapy. *Nat Med*. 2013;19(9):1178–1183.
43. Ni C, et al. Interferon-γ safeguards blood-brain barrier during experimental autoimmune encephalomyelitis. *Am J Pathol*. 2014;184(12):3308–3320.
44. Huang P, Duda DG, Jain RK, Fukumura D. Histopathologic findings and establishment of novel tumor lines from spontaneous tumors in FVB/N mice. *Comp Med*. 2008;58(3):253–263.
45. Pistner A, Belmonte S, Coulthard T, Blaxall B. Murine echocardiography and ultrasound imaging. *J Vis Exp*. 2010;(42):2100.
46. Peavey MC, et al. Three-dimensional high-frequency ultrasonography for early detection and characterization of embryo implantation site development in the mouse. *PLoS One*. 2017;12(1):e0169312.